Wind and Structures, Vol. 9, No. 5 (2006) 357-367
DOI: http://dx.doi.org/10.12989/was.2006.9.5.357

Mean pressure prediction for the case of 3D unsteady turbulent flow past isolated prismatic cylinder

V. Ramesh†, S. Vengadesan‡ and J.L. Narasimhan‡†

Department of Applied Mechanics, IIT Madras, Chennai-36, India
(Received October 20, 2005 Accepted, July 18, 2006)

Abstract. Unsteady 3D Reynolds Averaged Navier-Stokes (URANS) solver is used to simulate the turbulent flow past an isolated prismatic cylinder at Re=37,400. The aspect ratio of height to base width of the body is 5. The turbulence closure is achieved through a non-linear $k-\varepsilon$ model. The applicability of this model to predict unsteady forces associated with this flow is examined. The study shows that the present URANS solver with standard wall functions predicts all the major unsteady phenomena showing closer agreement with experiment. This investigation concludes that URANS simulations with the non-linear $k-\varepsilon$ model as a turbulence closure provides a promising alternative to LES with view to study flows having complex features.

Keywords: bluff body; non-linear turbulence model; URANS.

1. Introduction

Computational wind engineering (CWE) deals with the application of methodologies of Computational fluid dynamics (CFD) in the classical wind engineering and building aerodynamics. The flow of air influences the forces and moments on the structure. The modeling of flow conditions, complex building configurations, large area of model domain require huge and fine computational grids, large computer memory and time. Turbulence modeling plays an important role in simulation of such complex flows.

Direct numerical simulations (DNS) are possible only for flows with relatively low Reynolds numbers and further they are very costly. In Large-eddy simulations (LES) one resolves the large-scale turbulent motions and models the small-scale and is less expensive than DNS. LES can be applied to high Reynolds number flows when suitable near-wall mesh resolutions or approximations are used. Though this method is particularly suited for situations in which large-scale structures and mixing dominate the flow, it is yet to be used in practical situations (Spalart 2000). The methods that are used today for practical calculations are still largely based on solving the Reynolds-averaged Navier-Stokes (RANS) equations together with a statistical turbulence model. In CWE, simpler models like linear eddy viscosity models (EVMs) are still being used and the trend is going towards non-linear EVMs rather than to the numerically troublesome Reynolds-stress-equation

† M. S. Research Scholar
‡ Assistant Professor, Corresponding Author, E-mail: vengades@iitm.ac.in
‡† Professor

models. Further testing of these methods is necessary to determine which of the many different versions offers the best general prediction.

Considerable amount of literature exists on both experimental (Castro and Robbins 1977, Sakamoto and Arie 1982, Wu, *et al.* 2001, Becker, *et al.* 2002) and numerical studies (Murakami and Mochida 1988, Baskaran and Stathopoulos 1989, Zhang 1994, Meroney, *et al.* 1999, Oliveira and Younis 2000) dealing with the problem of flow past buildings. In most of the numerical studies reported so far, standard $k-\varepsilon$ model with ad-hoc modification or Reynolds stress models (RSM) are used. These models have deficiencies like over-prediction of turbulent kinetic energy or under-prediction of pressure in the case of standard $k-\varepsilon$ model and numerical stiffness and high computational cost in the case of RSM. Alternative way is to use non-linear models. These nonlinear EVMs are gaining interest as Unsteady Reynolds Navier-Stokes (URANS) simulation to predict the flows with gross unsteadiness owing to their computational time efficiency over LES. It is essential to study the features of the flow around such bluff bodies to estimate wind loads and the effects of interference between two or more bodies.

For this purpose, in the present work, numerical and experimental investigations are performed on an isolated three-dimensional square prismatic cylinder. The cylinder considered is of a square cross-section, the height (h) being 5 times the width (b). The experiments were performed in a boundary layer wind tunnel with 1/7th law velocity profile. In numerical predictions, the non-linear $k-\varepsilon$ turbulence model is used to solve the Unsteady Reynolds Averaged Navier-Stokes equations. To the best of our knowledge, no numerical work has been reported so far on three-dimensional turbulent flow simulation by non-linear model for the test case of high-rise buildings. The pressure distribution measured in the experiments is compared with that obtained by the numerical simulation and the model performance is ascertained.

2. Computational method

2.1. Basic equations

The ensemble averaged RANS equations for an incompressible and isothermal flow are Continuity equation:

$$\frac{\partial U_i}{\partial x_i} = 0 \tag{1}$$

Momentum equation:

$$\frac{\partial U_i}{\partial t} + \frac{\partial U_i U_j}{\partial x_j} = -\frac{1}{\rho}\frac{\partial p}{\partial x_i} + \frac{\partial(-\overline{u_i u_j})}{\partial x_j} + \nu\frac{\partial^2 U_i}{\partial x_j^2} \tag{2}$$

Due to ensemble averaging process, further unknowns are introduced to the momentum equations by means of Reynolds stresses $(-\overline{u_i u_j})$. In engineering flows, closure approximation using two-equation models (EVMs) for $-\overline{u_i u_j}$ have gained popularity due to their simplicity. In this paper, the study is confined to $k-\varepsilon$ model which employs additional transport equations for the turbulent kinetic energy k and its dissipation rate ε.

Transport equations for k and ε are given as

$$\frac{\partial k}{\partial t} + \frac{\partial k U_j}{\partial x_j} = -\overline{u_i u_j}\frac{\partial U_i}{\partial x_j} - \varepsilon + \frac{\partial}{\partial x_j}\left(\left(\frac{\nu_t}{\sigma_k} + \nu\right)\frac{\partial k}{\partial x_j}\right) \tag{3}$$

$$\frac{\partial \varepsilon}{\partial t} + \frac{\partial \varepsilon U_j}{\partial x_j} = -C_{\varepsilon 1}\frac{\varepsilon}{k}\overline{u_i u_j}\frac{\partial U_i}{\partial x_j} - C_{\varepsilon 2}\frac{\varepsilon^2}{k} + \frac{\partial}{\partial x_j}\left(\left(\frac{\nu_t}{\sigma_\varepsilon} + \nu\right)\frac{\partial \varepsilon}{\partial x_j}\right) \tag{4}$$

where, x_i is the spatial co-ordinate, t is the time, U is the averaged velocity, u_i is the fluctuating velocity, p is the averaged pressure, ρ is the fluid density, k is the turbulent kinetic energy, ε is the turbulent kinetic energy dissipation rate, ν_t is the eddy viscosity and ν is molecular kinematic viscosity.

2.2. The non-linear $k-\varepsilon$ (NLKE) model

In the standard $k-\varepsilon$ model, the Reynolds stresses are calculated by the linear relation proposed by Boussinesq as

$$-\overline{u_i u_j} = \nu_t S_{ij} - \frac{2}{3}k\delta_{ij} \tag{5}$$

where S_{ij} is the mean strain-rate tensor. It is well known that the standard $k-\varepsilon$ model does not take into account anisotropy effects and fails to represent the complex interaction mechanisms between Reynolds-stresses and mean velocity field. For example, the linear model fails to mimic the effects related to streamline curvature or secondary motion. These anisotropic effects can be predicted by introducing non-linear expression for the Reynolds stresses as given in the following expression

$$-\overline{u_i u_j} = \nu_t S_{ij} - \frac{2}{3}k\delta_{ij} + \left(\left(-\frac{k}{\varepsilon}\nu_t\right) \times \text{Nonlinear terms}\right) \tag{6}$$

General expression for non-linear terms is given as

$$\alpha_1(S_{il}\Omega_{lj} + \Omega_{il}S_{lj}) + \alpha_2\left(S_{il}S_{lj} - \frac{1}{3}S_{km}S_{mk}\delta_{ij}\right) + \alpha_3\left(\Omega_{il}\Omega_{lj} - \frac{1}{3}\Omega_{km}\Omega_{mk}\delta_{ij}\right) + \alpha_4\frac{k}{\varepsilon}(S_{kl}\Omega_{lj} + S_{kj}\Omega_{li})S_{kl}$$

$$+ \alpha_5\frac{k}{\varepsilon}\left(\Omega_{il}\Omega_{lm}S_{mj} + S_{il}\Omega_{lm}\Omega_{mj} + \frac{2}{3}S_{lm}\Omega_{mn}\Omega_{nl}\delta_{ij}\right) + \alpha_6\frac{k}{\varepsilon}(S_{il}S_{kl}S_{kl}) + \alpha_7\frac{k}{\varepsilon}(S_{ij}\Omega_{kl}\Omega_{kl}) \tag{7}$$

Coefficients (α_i $i = 1,7$) are determined through rapid distortion theory and the realizability principle.

In the present study, the non-linear coefficients considered are those proposed by Kimura and Hosoda (2003) for bluff body flows. In this model, previous experimental data is also considered for evaluating these coefficients. These are given as

$\alpha_1 = (C_3 - C_1)/4.0$; $\alpha_2 = (C_1 + C_2 + C_3)/4.0$; $\alpha_3 = (C_2 - C_1 - C_3)/4.0$;
$\alpha_4 = 0.02\, f_M(M)$, $\alpha_5 = 0$, $\alpha_6 = 0$, $\alpha_7 = 0$
where $C_1 = 0.4\, f_M(M)$, $C_2 = 0$, $C_3 = -0.13\, f_M(M)$ and

$$f_M(M) = (1 + 0.01M^2)^{-1},\ M = \max(S, \Omega),\ S = \frac{k}{\varepsilon}\sqrt{\frac{1}{2}\left(\frac{\partial U_i}{\partial x_j} + \frac{\partial U_j}{\partial x_i}\right)^2},\ \Omega = \frac{k}{\varepsilon}\sqrt{\frac{1}{2}\left(\frac{\partial U_i}{\partial x_j} - \frac{\partial U_j}{\partial x_i}\right)^2}$$

S is the strain rate parameter and Ω is the rotation parameter. In RANS models, the turbulent viscosity

ν_t is given by the expression $\nu_t = C_\mu \frac{k^2}{\varepsilon}$ and in the standard $k-\varepsilon$ model C_μ is set to a constant value of 0.09. It is known that this constant value does not satisfy the realizability constraint. In the present model, C_μ is expressed as a function of S and Ω and is given by

$$C_\mu = \min\left(0.09, \frac{0.3}{1 + 0.09M^2}\right). \tag{8}$$

3. Test case and numerical strategies

3.1. Experimental study

The flow over a finite square prismatic cylinder with height h and width b is predicted and studied as a test case. The model dimensions used are $b = 60$ mm and $h = 300$ mm, so that the aspect ratio is $h/b = 5.0$, which is classified as high-rise structure. The measurements were carried out in the low speed, straight-through, blower-type boundary layer wind tunnel of Fluid Mechanics Laboratory, Indian Institute of Technology Madras. Following Cowdrey's (1967) procedure, at the end of the contraction, a grid of smooth mild steel rods, each of 10 mm diameter with varying spacing is provided so as to obtain at the inlet of the test section a 1/7th power law boundary layer type velocity profile. The test section has a square cross-section of side 610 mm and a length of 1975 mm. The power law velocity distribution is first observed at a distance of 450 mm from the grid in the stream-wise (x) direction and is found to be maintained constant for the next 1000 mm in the test section. The mean velocity distribution in the test section of the wind tunnel has been measured by a standard Pitot-static probe of 3 mm outer diameter. Check for two-dimensionality of the flow in test-section of the wind tunnel and self-similarity of the velocity profile have also been performed. The pressure taps on the surface of the test body are connected to various ports of a scanning box (FC091; make: Furness Controls, UK). The output of this is connected to a micro-manometer (FC012; make: Furness Controls, UK). These pressure readings of the transducer are digitized by connecting the output of the manometer to a personal computer through A/D card. For time-averaged mean quantities of pressure, the instantaneous values are collected for 20 sec. at a sampling rate of 20 Hz. These values are averaged to get the mean static pressure at a point. The experiment was carried out at a free stream velocity U_∞ of 9.34 m/s and the Reynolds number Re based on the free stream velocity U_∞ and the width b of the body is 3.74×10^4. This experimental facility with similar measurement arrangements have been used earlier for many studies (Tulapurkara, *et al.* 2005). More details on experiments are available in Ramesh (2005).

3.2. Validation

A commercial package FLUENT 6.1 has been used to solve the basic governing equations for velocities and turbulent quantities. The equations were discretized using the finite volume method on a collocated grid in fully implicit form. The second order upwind differencing scheme was used for convective terms and also the terms in equations for turbulent quantities, k and ε. Central differencing scheme was adopted for solving diffusion terms. Fully implicit second-order backward stencil (Berth and Jespersen 1989) scheme was used for time integration of each equation. The SIMPLE algorithm was used for coupling the pressure and velocity terms. The present non-linear

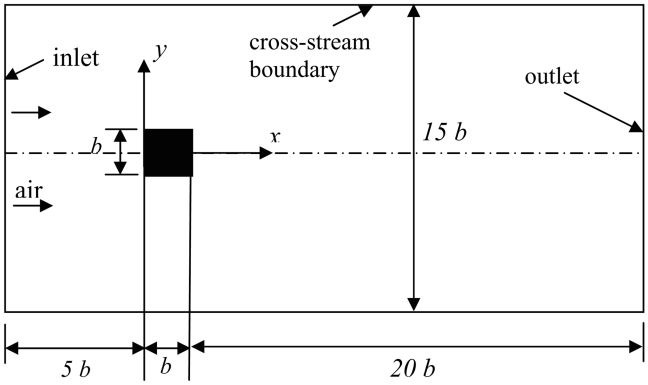

Fig. 1 Schematic representation of the computational domain for an isolated square prismatic cylinder

model is incorporated in FLUENT through User Defined Functions (UDFs). The non-linear stress term is added as source term in the equations for k and ε and in the momentum equation. The turbulent viscosity is also made to vary according to Eq. (8) through UDFs. The nonlinear model incorporated in FLUENT for computation is validated against the standard bench mark experimental data of turbulent flow past a square cylinder at $Re = 22{,}000$ (Lyn, *et al.* 1995) and the details of which are reported at Ramesh, *et al.* (2006). It is concluded from this validation case that the present non-linear $k-\varepsilon$ model captures the mean and unsteady characteristics of the flow better than other RANS models. Due to these encouraging performance capabilities, the same non-linear model (NLKE) is used to study the flow over an isolated square prismatic cylinder of finite height.

3.3. Discretization schemes and computational domain

The schematic diagram of computational domain is shown in Fig. 1. Structured grid in Cartesian coordinates is chosen, where x-axis is along the streamwise direction, y-axis is in the cross-stream direction and z-axis is in the vertical direction, normal to the x-y plane. The height of the computational domain is fixed to $10b$ to maintain the depth of immersion of the cylinder in the boundary layer exactly the same way as in the experiment conducted in the boundary layer wind tunnel. It has been shown by Sakamoto and Arie (1982) that the amount of immersion and the presence of wall in the spanwise direction will affect the pressure distribution on the roof.

At inlet, a boundary layer profile as seen at $x = 450$ mm from the grid in the wind tunnel is prescribed with turbulence intensity, $I = 5\%$, which is observed in most part along the spanwise direction. Convective boundary condition is specified at the outlet. Symmetry boundary condition is adopted at the cross-stream direction. No-slip boundary condition is applied at the top and bottom (spanwise) boundaries ($z = 0$ and $z = 10b$) and also specified on the surface of the cylinder. Standard wall functions of Launder and Spalding (1974) are used here to bridge the viscosity affected near-wall region and the fully turbulent outer region. The solver and discretization schemes used here are the same as those applied for the bench mark case discussed in 3.2.

4. Results and discussion

The numerical solution is started with prescribed initial and boundary conditions, and calculations

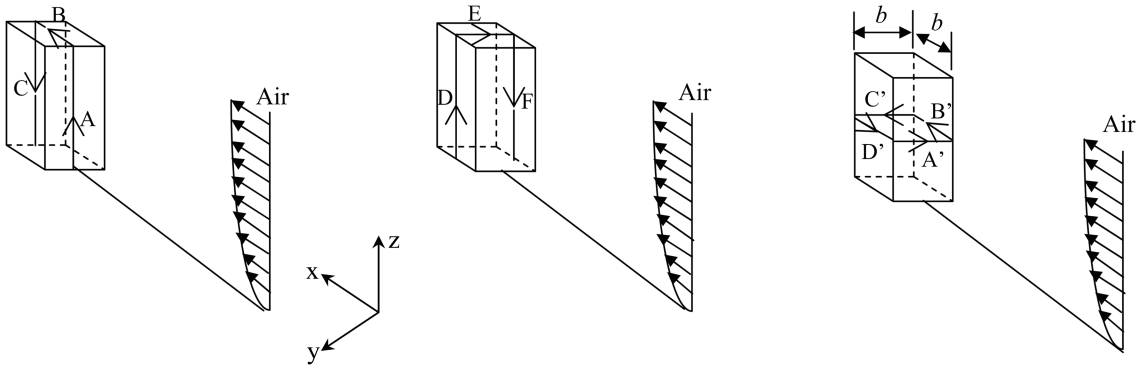

(a) Faces A, B and C **(b) Faces D, E and F** **(c) Faces A', B', C' and D'**

Fig. 2 Naming conventions

are advanced with an increment in time of $\delta t = 0.001$ s. Calculations are allowed to march in time, until the vortex shedding attains periodic nature, which is ascertained by observing the variation of lift coefficient as a periodic function of time. The number of time steps for one vortex shedding cycle after periodicity is attained came to be around 80 to 85. The frequency is calculated from the FFT of the time varying signal of C_l. Within each time step 30 iterations were given. The convergence levels were constant even if the iteration number was more. Once the flow becomes periodic, mean quantities are obtained by averaging the instantaneous quantities over ten vortex shedding cycles. Results obtained by the present simulations with the NLKE model are presented and compared with experimental data and discussed in this section.

The naming conventions used for different faces of the prismatic isolated cylinders are shown in Fig. 2. In Fig. 2(a), the front face of the cylinders is represented by A in the vertical direction from bottom to top; then on the top face (roof) as shown by B in the flow direction and on the rear face as C from top to bottom in vertical direction. In Fig. 2(b), D and F show the vertical direction on either side of the cylinder and E is in the cross-stream direction on top of the cylinder. In Fig. 2(c), A' and C' are in the cross-stream direction on front and rear faces of the cylinder, while B' and D' are along the side faces of the cylinder.

Grid independence tests were conducted by varying the first mesh point from the body. For the two grids considered, the distance of the first grid point (δy) from the wall is taken as $0.01b$ and $0.02b$ respectively and the number of grid points for the two grids are $127 \times 90 \times 65$ and $112 \times 70 \times 50$ respectively. The pressure distribution on the different faces of the cylinder is shown in Fig. 3. Since the variation in the results for the two grids is quite small, except near the base of the cylinder for the rear and side faces (along C and F), the grid with $\delta y = 0.02\ b$ and with $112 \times 70 \times 50$ grid points is considered for further calculations.

Fig. 4 shows the variation of mean C_p on different faces for the case of isolated body. The results predicted by the present non-linear $k-\varepsilon$ model are compared with those of the present experimental study. From Fig. 4(a) we can see that the present NLKE model predicts the stagnation point on the front face. This could probably due to the fact that the model satisfies the realizability constraint by variation of C_μ as per Eq. (7). On the front face, in vertical direction along A, the stagnation point at $z = 0.8\ h$ is predicted by the NLKE model as in the experiments. The present model also captures the secondary vortex formation at the bottom of the front face which is seen by the dip in the C_p value at about $z = 0.08\ h$. The point where the minimum C_p occurs is a nodal point, where the flow

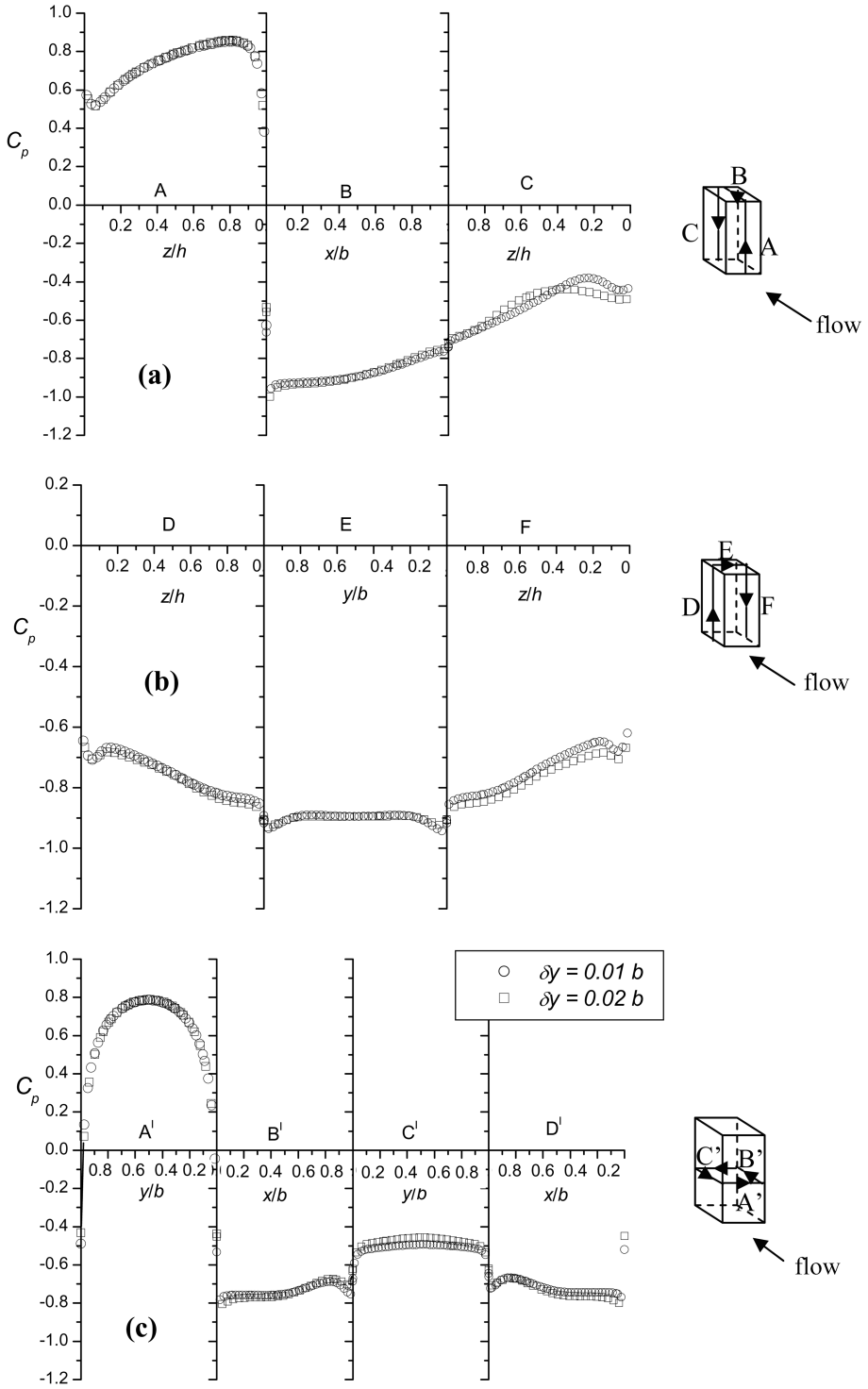

Fig. 3 C_p distribution on different faces of the isolated prismatic cylinder for two different grids considered

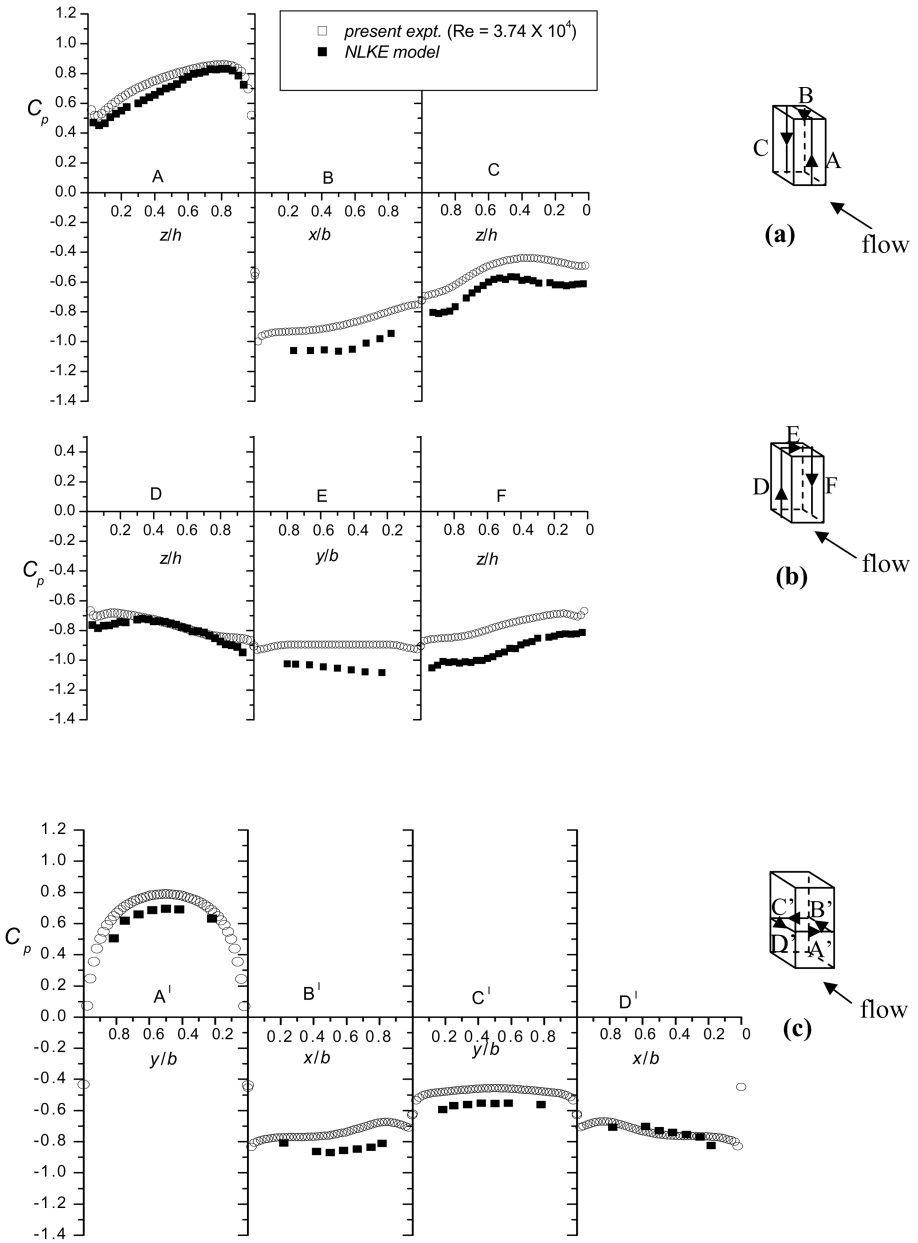

Fig. 4 Comparison of C_p on different faces by experiment and numerical simulation for an isolated prismatic cylinder

diverts in both forward and downward direction. The RNG $k-\varepsilon$ fails to predict this phenomenon. On the roof, along the direction B, the flow separates at the leading edge and hence there is higher suction pressure at that point and the suction pressure reduces towards the trailing edge with a constant gradient. Hence there is no reattachment on the roof along B. On the rear face C, the downward curving flow which is separated from the roof, forms a large recirculation bubble in the

wake (behind the body). The flow separated from the sides also curves inwards making the flow interaction three dimensional and complex in the wake. Due to this, the suction pressure decreases with a steep gradient and the gradient becomes zero at about $z = 0.4\ h$ and there onwards, the pressure remains almost constant. The recirculation bubble reattaches on the rear face at this point. This is predicted better by the NLKE model and also can be observed from the experiments. On the side face along D, the suction pressure increases steeply towards the top, as seen in Fig. 4(b). The increase in suction pressure at the top of the face is due to the relatively high speed flow separating from the side edges and the front face. Along the face E, which is also on roof and in cross-stream direction, there is a constant suction pressure along the face except near the edges. Along the face F, the trend is similar to that of face D.

On the front face along the horizontal direction A', the C_p value is maximum at the centre of the face because of stagnation and decreases towards the edges, as shown in Fig. 4(c). This is due to the division of the flow in the middle and its movement on either side of the cylinder in the horizontal plane. On the side face along B', the C_p is almost constant at –0.8, the suction pressure slightly decreases towards the trailing edge as the shear layer starts curving into the wake. The C_p value on the rear face along C' is constant, as the suction pressure in the near wake is constant in the horizontal plane due to formation of alternating vortices. The C_p value on the side face along D' is the same as the other side face along B'. From this figure, it can be noticed that the present NLKE model predicts fairly well.

Fig. 5 shows the velocity vectors in the central vertical plane of the cylinder. The regions

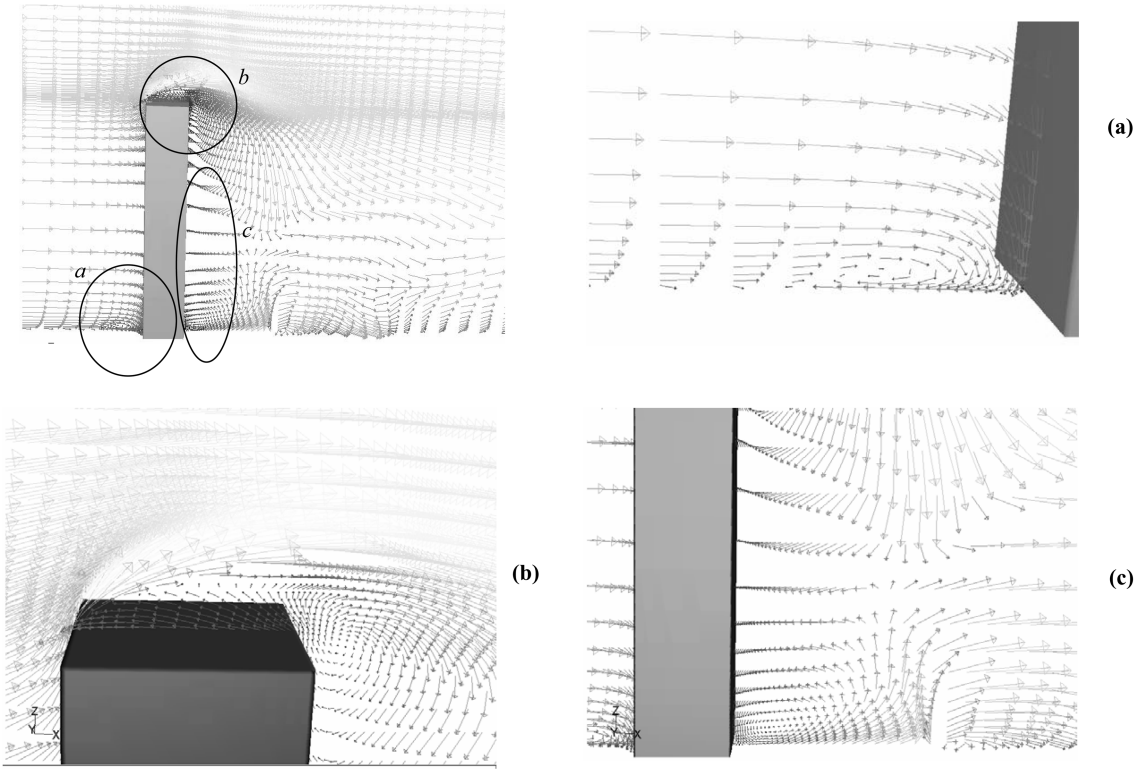

Fig. 5 Velocity vectors in the central vertical plane showing the important flow phenomena around the prismatic cylinder

encircled in the figure are enlarged and shown in Figs. 5(a), (b), and (c). In region (a), the bottom region of the front face, where the secondary vortex formation is captured by the NLKE model, is shown. In region (b), the roof portion, where there is no reattachment of the separated shear layer from the front top edge can be observed. The formation of recirculation bubble at the back can also be seen. In region (c), the bottom half of the rear faces is shown. The reattachment of the recirculation bubble on to the rear face can be seen. The remaining flow moves downwards and forms another vortex which moves in the downstream direction. These observations confirm that the NLKE model captures the entire major steady and unsteady phenomena better than other unsteady RANS models.

All the calculations were performed by Pentium-IV 3.0 GHz processor. 1GB SDRAM. It took 3 days for the solution to become periodic and two days for ten vortex shedding cycles. The CPU time was not calculated but apart from the system programs, FLUENT was the only major application running program. It was observed that FLUENT used more than 95% of CPU utilization. From the above, it is observed that the NLKE model predicts the major and unsteady flow phenomena with reasonable accuracy better than the linear eddy viscosity models like RNG $k-\varepsilon$ model, with limited computational resources than that would have been required by LES for the same test flow case.

5. Conclusions

An unsteady computation of turbulent flow past an isolated three-dimensional prismatic cylinder is performed using a non-linear $k-\varepsilon$ model of turbulence. The stagnation point at the front face is better predicted when compared with that by the standard $k-\varepsilon$ model. Pressure forces acting on the surfaces of cylinder are also predicted better and found to be matching with those of experiment. Explanation of unsteady phenomena associated very well with this type of flow has also been made through prediction of velocity vectors and lift and drag forces. Considering the computational cost required by LES, the present model serves as a viable alternative to simulate such kind of unsteady flows and estimate wind loads on buildings, and study effects due to interference of two or more bodies.

References

Baskaran, A. and Stathopoulos, T. (1989), "Computational evaluation of wind effects on buildings", *Buildings and Environ.*, **24** (4), 325-333.

Becker, S., Lienhart, H., and Durst, F. (2002), "Flow around three-dimensional obstacles in boundary layers", *J. Wind Eng. Ind. Aerodyn.*, **90**, 265-279.

Berth, T. J. and Jespersen, D. (1989), "The design and application of upwind schemes for unstructured meshes", *Technical Report AIAA-89-0366*, AIAA 27th Aerospace Sciences Meeting, Reno, Nevada.

Castro, I. P. and Robbins, A. G. (1977), "The flow around a surface mounted cube in uniform and turbulent streams", *J. Fluid Mech.*, **79**, 307-335.

Cowdrey, C. F. (1967), "A simple method for the design of wind tunnel velocity profile grids", *National Physical Laboratory*, Teddington, UK, Aerodyn. Division, Note 1055.

Kimura, I. and Hosoda, T. (2003), "A non-linear $k-\varepsilon$ model with realizability for prediction of flows around bluff bodies", *Int. J. Numerical Methods in Fluids*, **42**, 817-837.

Launder, B. E. and Spalding, D. B. (1974), "The numerical computation of turbulent flows", *Comp. Methods in Appl. Mech. Eng.*, **3**, 269-289.

Lyn, D. A., Einav, S., Rodi, W., and Park, J. H. (1995), "A laser-doppler velocimetry study of ensemble-

averaged characteristics of a square cylinder", *J. Fluid Mech.*, **304**, 285-319.
Meroney, R., Bernd, N., Leitl M., Rafailidis, S., and Schatzmann, M. (1999), "Wind-tunnel and numerical modeling of flow and dispersion about several building shapes", *J. Wind Eng. Ind. Aerodyn.*, **81**, 333-345.
Murakami, S. and Mochida, A. (1988), "Three-dimensional numerical simulation of turbulent flow around buildings using $k-\varepsilon$ turbulence model", *Buildings and Environ*, **24**(1), 51-64.
Oliveria, P. J. and Younis, B. A. (2000), "On the prediction of turbulent flow around full-scale buildings", *J. Wind Eng. Ind. Aerodyn.*, **86**, 203-220.
Ramesh, V. (2005), "Study of interference effects on three-dimensional bluff bodies in staggered arrangement", M. S. Thesis, IIT Madras.
Ramesh, V., Vengadesan, S., and Lakshminarasimhan, J. (2006), "3D unsteady RANS simulation of turbulent flow over bluff body by non-linear model", *Int. J. Numer. Meth. Heat Fluid Flow*, **16**, 660-673.
Sakamoto, H. and Arie, M. (1982), "Flow around a cubic body immersed in a turbulent boundary layer", *J. Wind Eng. Ind. Aerodyn.*, **9**, 275-293.
Spalart, P. R. (2000), 'Strategies for turbulence modeling and simulations", *Int. J. Heat and Fluid Flow*, **21**, 252-263.
Tulapurkara, E. G., Gowda, B. H. L., and Chaukar, J. S. (2005), "Mean velocity field around prismatic bodies in tandem arrangement", *J. Wind Eng. Ind. Aerodyn.*, **93**, 777-796.
Wu, F., Sarkar, P. P., Mehta, K. C., and Zhao, Z. (2001), "Influence of incident wind turbulence on pressure fluctuations near flat roof corners", *J. Wind Eng. Ind. Aerodyn.*, **89**, 403-420.
Zhang, C. X. (1994), "Numerical predictions of turbulent recirculating flows with a $k-\varepsilon$ model", *J. Wind Eng. Ind. Aerodyn.*, **51**, 177-201.

CC